ARTICLES
PUBLISHED ONLINE: 14 MARCH 2010 | DOI: 10.1038/NCHEM.581
nature chemistry

Face-directed self-assembly of an electronically active Archimedean polyoxometalate architecture

Scott G. Mitchell, Carsten Streb, Haralampos N. Miras, Thomas Boyd, De-Liang Long and Leroy Cronin*

The convergent assembly of metal–organic frameworks has enabled the design of porous materials using a structural building unit approach, but functional systems incorporating pre-assembled structural building unit 'pore' openings are rare. Here, we show that the face-directed assembly of a ring-shaped macrocyclic polyoxometalate structural building unit, $\{P_8W_{48}O_{184}\}^{40-}$ with an integrated 1-nm pore as an 'aperture synthon', with manganese linkers yields a vast three-dimensional extended framework architecture based on a truncated cuboctahedron. The 1-nm-diameter entrance pores of the $\{P_8W_{48}O_{184}\}^{40-}$ structural building unit lead to approximately spherical 7.24-nm^3 cavities containing exchangeable alkali-metal cations that can be replaced by transition-metal ions through a cation exchange process. Control over this process can be exerted by either electrochemically switching the overall framework charge by manipulating the oxidation state of the manganese linker ions, or by physically gating the pores with large organic cations, thus demonstrating how metal–organic framework-like structures with integrated pores and new physical properties can be assembled.

The assembly and control of nanospaces with pre-defined internal environments[1] are important for catalysis[2], inclusion phenomena[3,4] and molecular recognition[5]. In particular, the development of modular materials for these purposes, including metal–organic cages[6] and metal–organic frameworks[7] (MOFs) and related materials[8], has hinged on the coordination-driven design strategy of combining multitopic inorganic linking nodes to organic ligands. This approach, often described as the structural building unit (SBU) approach, has allowed the design of highly functional 'smart' materials[9], and has enabled a reliable modular building-block approach to develop rapidly, in an unparalleled fashion, over the last decade[10]. One critical aspect of this approach is the topology of the resultant networks. Judicious selection of appropriate nodes and linkers using design principles defined using symmetry arguments results in an assortment of topologically related architectures with high geometric ordering[11]. Importantly, the design strategies that have emerged generally make use of inorganic SBUs as rigid polyhedra, which allow for a higher degree of predictability in the outcome of resulting molecular topologies. However, these units do not themselves normally incorporate units with a pore; normally the pore openings are constructed as a result of the framework assembly. Despite the unparalleled success[12] of this approach in designing MOFs, the reliable design of all inorganic frameworks from first principles has not yet been successful, partly due to the difficultly in defining the SBUs[13].

Polyoxometalate (POM)-based materials, which represent a well-defined library of anionic molecular inorganic building blocks[14] with an enormous range of physical and chemical properties[15,16], are prime candidates[17] for the design and construction of tailored framework materials[18]. Architectures built from all-inorganic molecular precursors such as these are of great interest and, importantly, many cyclic and 'wheel shaped' POM molecules can be synthesized[19], thereby offering the possibility of designing frameworks with integrated pores. For example, a range of POM-based 'aperture synthons' with pore sizes ranging from 0.5 to 3 nm are available. These compounds display a diverse range of physical and chemical properties with relevance to areas such as catalysis[16], biology[20] and materials science[21,22]. Therefore POM clusters potentially define a vast library of readily available and controllable SBUs[23], because these high-nuclearity metal oxides can be interconnected by electrophilic[24] linkers or electrostatic interactions[25], giving a key architectural design principle for the systematic development of functional inorganic frameworks. As such, inorganic POM-based frameworks offer significant potential for the formation of new types of porous materials that combine the thermal stability of zeolites[26] and mesoporous silicas[27] with the sophistication and versatility of MOFs and of course, incorporate the almost unmatched range of physical properties associated with POMs[14].

We present an open framework material designed from highly anionic molecular building blocks with integrated pores: the crown-type POM $\{P_8W_{48}O_{184}\}^{40-}$, which incorporates a 1-nm pore, is used as an SBU, which forms the basis of the molecular scaffold[28–30]. The combination of this fragment with redox-switchable electrophilic linkers forms an accessible open framework nanocube-based architecture, $K_{18}Li_6[Mn_8(H_2O)_{48}P_8W_{48}O_{184}]\cdot 108H_2O$ **1** (Fig. 1). To explore the functionality of this material we present quantitative cation exchange studies that detail the uptake of cations from solution into the network channels and cavities. Importantly, this cation exchange process is tunable with respect to the electronic state of **1**: by oxidizing the manganese linkers from 2+ to 3+ it is possible to electrochemically switch the cation exchange properties of the material. Furthermore, one additional way of exerting control over the cation exchange properties of the material is by blocking ('gating') the pores present in **1**, defined by the $\{P_8W_{48}O_{184}\}^{40-}$ linked cluster anions, with a large organic molecule, such as 2,4,6-*tris*(dimethylaminomethyl)phenol (TDAMP), thus preventing entry of cations into the cavities of the framework.

$K_{18}Li_6[Mn_8(H_2O)_{48}P_8W_{48}O_{184}]\cdot 108H_2O$ **1** was synthesized by means of a carefully optimized set of experimental procedures and crystallization conditions. These variable synthetic parameters, including pH, temperature, solvent composition and concentration, ensure the ligation of manganese centres onto the outer regions of $\{P_8W_{48}O_{184}\}^{40-}$ fragments, thereby facilitating the necessary

WestCHEM, Department of Chemistry, The University of Glasgow, University Avenue, Glasgow G12 8QQ, UK. *e-mail: l.cronin@chem.gla.ac.uk

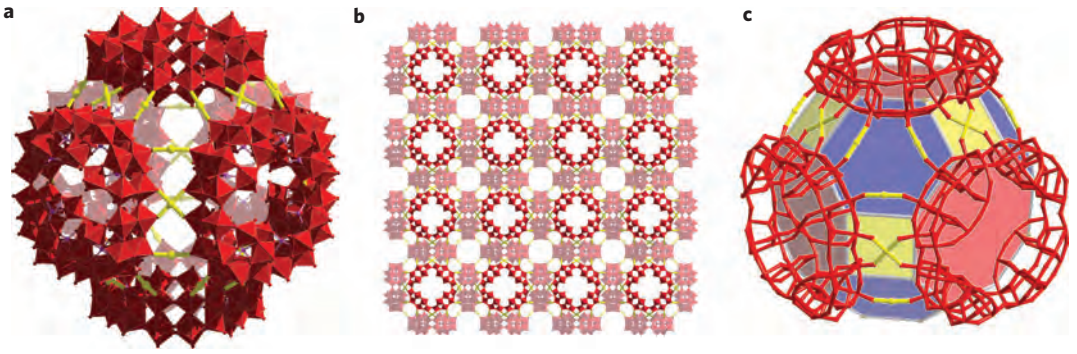

Figure 1 | Open framework material 1 is built from the face-directed assembly of a highly anionic $\{P_8W_{48}O_{184}\}^{40-}$ molecular building unit, which incorporates a 1-nm pore, combined with electrophilic manganese linkers, which are redox-switchable. a–c, The highly accessible three-dimensional network **1** crystallizes in cubic space group *Pm-3m*: packing of manganese-linked $\{P_8W_{48}O_{184}\}^{40-}$ clusters forming a truncated cuboctahedron (**a**), crystal packing of $[Mn_8(H_2O)_{48}P_8W_{48}O_{184}]^{24-}$ (**1a**) along the crystallographic *a* axis (**b**), packing of manganese-linked $\{P_8W_{48}O_{184}\}^{40-}$ clusters around a truncated cuboctahedron (**c**). Red polyhedral, WO_6; red spheres, oxygen; yellow spheres, manganese; pink spheres, phosphorus. All alkali metal cations and solvent water molecules have been omitted for clarity.

connectivity for open framework architectures. **1** crystallizes as yellow cubic crystals and has been fully characterized by single-crystal X-ray crystallography, powder X-ray diffraction (PXRD), redox titrations and thermogravimetric analysis (TGA), as well as flame photometry (FP), Fourier-transform infrared (FT-IR), ultraviolet-visible (UV-Vis) and flame atomic absorption spectroscopy (FAAS).

The principle building unit of **1** is best described as a 'truncated cuboctahedron' (or great rhombicuboctahedron); put simply, the molecular panelling of $\{P_8W_{48}O_{184}\}^{40-}$ units into the network can essentially be viewed as cubic (Figs 1,2; see also Supplementary Figs S17–S20), a topology shared by several other notable materials. Strikingly, this topology is analogous to that of the prominent LTA Zeolite framework[26], because both frameworks crystallize in the cubic *Pm-3m* space group and differ only in the tiling round the central cuboctahedral cavity.

The high order of packing of **1** can be directly attributed to the number and location of Mn(II) centres that have been unambiguously determined to be in the Mn(II) oxidation state. Because each $\{P_8W_{48}O_{184}\}^{40-}$ fragment is linked to eight others by multiple {Mn–O–W} coordination bonds, an isolated $\{P_8W_{48}O_{184}\}^{40-}$ unit has a total of 24 manganese atoms located on its outer edges; however, owing to the cubic sharing nature of the architecture, eight Mn(II) atoms are associated with each $\{P_8W_{48}O_{184}\}^{40-}$ unit ($[Mn_8(H_2O)_{48}P_8W_{48}O_{184}]^{24-}$, **1a**) in the framework (Fig. 2). Importantly, the manganese atoms not only direct the structure of the resulting framework, but also impart important electrochemical properties to the material.

The manganese-fused $\{P_8W_{48}O_{184}\}^{40-}$ anions form a truncated cuboctahedron-based framework with large internal voids of ~27% of the unit cell volume (Figs 1,2; see also Supplementary Fig. S17). Consequently, the crystal lattice superstructure of **1** can be conceptualized as stacked 'empty' boxes. These approximately spherical voids have an internal diameter of ~2.4 nm (that is, a void volume of ~7.24 nm^3) and are accessible through the integrated pores of the six surrounding $\{P_8W_{48}O_{184}\}^{40-}$ anions. Importantly, this cavity (inside each truncated cuboctahedron 'box') is free of heavy metal atoms and, in addition to solvent water molecules, contains only the alkali-metal cations K^+ and Li^+. Because these cavities are accessible through the ring openings defined by the $\{P_8W_{48}O_{184}\}^{40-}$ units (essentially operating as pores), the cation exchange properties of the material could be monitored through facile cation uptake experiments. The studies reported herein detail the exchange of K^+ and Li^+ for *d*-block transition-metal cations, for example Cu^{2+}, Co^{2+} and Ni^{2+}; however, inspired by previous work[30], we gave particular attention to Cu^{2+}. This is because small

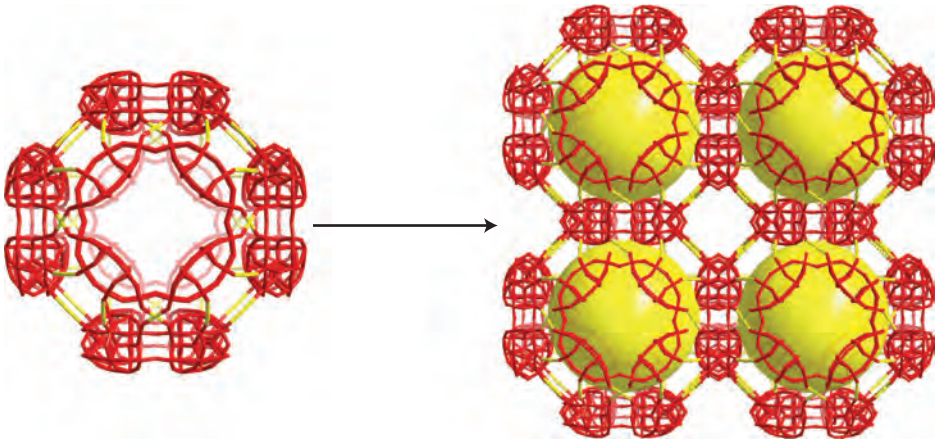

Figure 2 | Face-directed assembly of six $\{P_8W_{48}O_{184}\}^{40-}$ heteropolyanions through multiple {Mn–O–W} bonds along all axes, giving rise to a geometrically well-defined Archimedean solid: the truncated cuboctahedron. The geometrical arrangement of these fragments into the three-dimensional scaffold is shown, where yellow spheres represent the approximately spherical void space (~7.24 nm^3) within the cavity of each cuboctahedral building unit. Red wires, WO_x; yellow wires, MnO_x. All alkali-metal cations and solvent water molecules have been omitted for clarity.

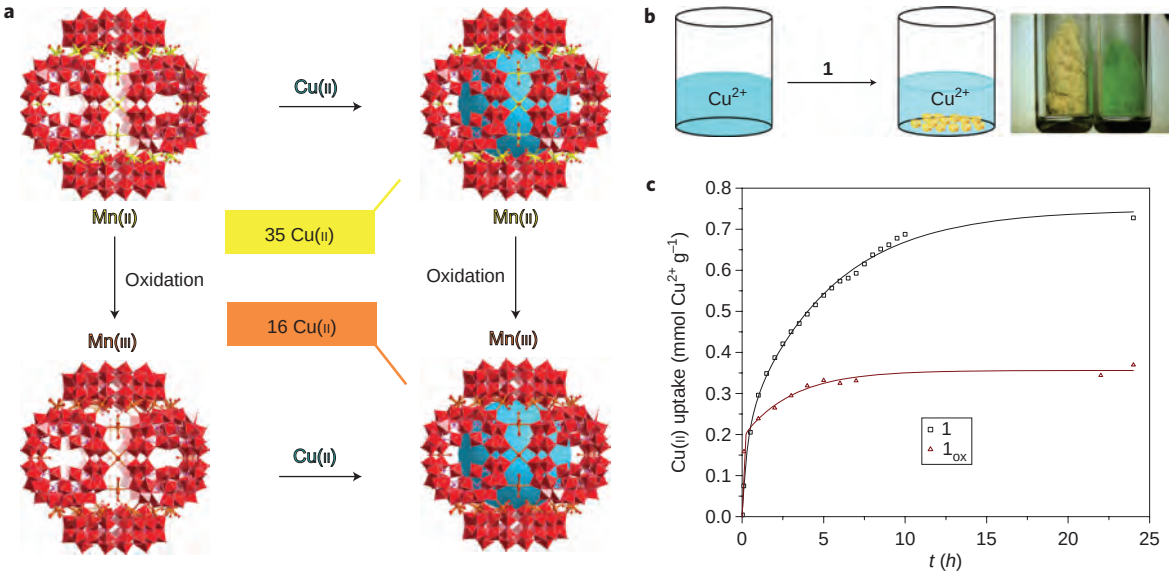

Figure 3 | UV spectrophotometric exchange experiments were used to establish the cation exchange capabilities of the solvent-accessible voids of 1 over a 24-h period. This figure summarizes the exchange study of $Cu^{II}(NO_3)_2{\cdot}3H_2O$ plus $[Mn_8(H_2O)_{48}P_8W_{48}O_{184}]^{24-}$ (**1a**) and oxidized (**1a**$_{ox}$). Elemental analysis and UV spectroscopic studies show that Cu^{2+} replaces K^+ and Li^+ in the channels and cavities of **1. a**, General experimental scheme for the cation exchange experiments and the principal results. **b**, General experimental procedure, complete with a photograph showing the visual observation of Cu(II) uptake into single crystals of **1. c**, Plot of uptake of Cu(II) into the cavities of **1** and **1**$_{ox}$ over a 24-h period. For **1** this corresponds to an uptake of 0.73 mmol Cu^{2+} per gram of **1**; for oxidized **1**$_{ox}$ this corresponds to 0.37 mmol Cu^{2+} per gram of **1**$_{ox}$ (~50% difference between the two redox phases: **1** to **1**$_{ox}$).

guest molecule exchange analyses, when coupled with PXRD, are useful as preliminary independent demonstrations of the functionality and integrity of an open-framework material[9].

Photometric experiments were used to establish the cation uptake capabilities of the solvent-accessible voids of **1** over a 24-h period. Cu(II) was used as a suitable probe for exchange experiments based on its size, stability and UV spectroscopic profile. In this instance, Cu(II) exchanges with the K^+ and Li^+ cations in the channels and cavities of **1**. Subsequent elemental and spectroscopic analyses of fresh crystals of **1** soaked in a solution of Cu(II) ions showed that freshly isolated crystals of **1** can take up 0.73 mmol of Cu(II) per gram of **1**, which represents approximately 35 Cu(II) ions per truncated cuboctahedron (Fig. 3; see also Supplementary Figs S7,S15). An X-ray powder diffraction comparison of **1** before and after exchange experiments indicates that the main structural features of the cubic framework are retained after Cu(II) uptake (Supplementary Fig. S3), and heating the material to framework collapse (>450 °C) renders the material inactive with respect to cation exchange reactions. Importantly, UV analyses show no evidence of leaching of Mn(II) ions from the framework architecture into solution during exchange studies, and Cu(II) exchange into the material was observed visually as the crystals changed colour from bright yellow to light blue (Fig. 1; see also Supplementary Fig. S8).

To gain greater control over the chemical reactivity and porosity of **1**, we reasoned that the oxidation of Mn(II) centres may decrease uptake by decreasing the overall negative charge on the framework. Oxidizing the Mn(II) centres involved the direct exposure of **1** to an ethanolic mixture of a suitable oxidizing agent, such as *meta*-chloroperoxybenzoic acid (mCPBA). On exposure to the oxidant, crystals of the material were immediately visually observed to change colour from bright yellow to light brown (dark brown over several hours), while at the same time retaining their distinctive cubic shape. PXRD and TGA confirmed the structural integrity of **1** after oxidation (Supplementary Figs S3,S12) and FAAS elemental analysis showed a reduction in K^+ and Li^+ concentration (in compensation for the reduction in negative charge of the framework), but there was no change in the concentration of tungsten or manganese in the material (Supplementary Section 5).

The resulting effect of increasing the oxidation state of the manganese atoms from Mn(II) to Mn(III) (framework **1** to **1**$_{ox}$, respectively) lowers the overall negative charge on the framework and consequently reduces the ability of the framework to take up cations from solution. This was proven by subjecting **1**$_{ox}$ to analogous uptake studies and, using the same UV photometric studies, the oxidized cluster **1**$_{ox}$ was capable of exchanging in 0.37 mmol Cu(II) per gram of **1**, representing approximately 16 Cu(II) per truncated cuboctahedron. Comparing the exchange properties of **1**$_{ox}$ with native **1** (the results of which can be seen in Fig. 3), a difference of ~50% is observed. In addition to independent Cu(II) uptake experiments on **1** and **1**$_{ox}$, it was possible to perform *in situ* oxidation of the manganese atoms during Cu(II) uptake, allowing us to direct the exchange properties from **1** towards **1**$_{ox}$ (Supplementary Fig. S10). Experimentally, during Cu(II) uptake into **1**, oxidizing agent was added to oxidize manganese linkers from Mn(II) to Mn(III) and an instant change in the pattern of the Cu(II) exchange experiment was observed. On oxidizing the manganese centres, the charge on the framework dropped and Cu(II) was released, settling finally on an amount of Cu(II) comparable to that observed for **1**$_{ox}$ (Supplementary Figs S7, S10). Thus we observe the transformation of **1** to **1**$_{ox}$ spectroscopically during the uptake of Cu(II) into the framework.

So far we have focused our efforts primarily on Cu(II) uptake; however, we have also observed analogous exchange of other cationic 3*d* transition-metal ions, small organic molecules and aromatic organic amines. Also, pre-soaking **1** in an ethanolic solution of organic molecules before Cu(II) cation exchange studies had significant effects on the outcome of our cation exchange studies. Compound **1** was soaked in a concentrated solution of a small organic molecule, 2,4,6-triaminopyrimidine (TAPI); UV photometric and NMR studies show the diffusion of organic molecule into the pores and cavities of **1**. Subsequently, TAPI-doped crystals were transferred into an ethanolic solution of Cu(II) ions, leading to the initial observation of a significantly reduced Cu(II) exchange in comparison to that observed for native **1**. However, because the concentration of Cu(II) ions was considerably higher than that of the TAPI associated with **1**, it took only 2–3 h for the uptake of Cu(II)

ions to become apparent as they found their way into the cavities of **1** and exchanged out the TAPI (Supplementary Fig. S15). Although we have observed that small organic molecules can enter the network cavities through the entrance pores in the $\{P_8W_{48}O_{184}\}^{40-}$ cluster, our results show that organic molecules with van der Waals radii larger than the pores are excluded from the framework based on their size. Consequently, for molecules such as TDAMP, the electrostatic interaction between the organic molecule and the entrance causes them to effectively function as gates to the $\{P_8W_{48}O_{184}\}^{40-}$ pores[13], thereby blocking entrance to the internal cavities (Supplementary Fig. S16). The effect of doping **1** with TDAMP before Cu(II) exchange studies led to a dramatic reduction in the exchange of Cu(II) ions, resulting in an uptake of only ~12 Cu(II) ions per truncated cuboctahedron of **1** (compared with the uptake of 35 Cu(II) ions observed for the native compound, **1**).

Conclusions

The face-directed self-assembly of this novel inorganic polyhedral nanocube-based framework, built from well-defined molecular inorganic parts, demonstrates that cyclic SBUs with intrinsic holes can be used for the design of functional inorganic framework materials. The physical properties of the highly anionic and porous SBU, $\{P_8W_{48}O_{184}\}^{40-}$, and the electrochemical aspects of the redox-switchable Mn(II) linkers both impart important characteristics on **1**. The net effect is a robust electrochemically switchable open framework material with the ability to controllably take up small molecules. We are at present working towards establishing the general design process for all-inorganic framework materials based on related molecular metal oxide SBUs and further studies aim to investigate the catalytic, sensing and guest exchange capabilities of **1** in more detail.

Methods

All chemicals and solvents were of analytical grade (Sigma Aldrich) and were used as supplied, without further purification. $K_{28}Li_5[H_7P_8W_{48}O_{184}]\cdot 92H_2O$ was synthesized from a modified method adapted from the original $\{P_8W_{48}O_{184}\}^{40-}$ paper published by Contant and Tézé[28].

Single-crystal X-ray diffraction. Suitable single crystals of **1** were selected and mounted onto the end of a thin glass fibre using Fomblin oil. X-ray diffraction intensity data for compound **1** were collected using an Oxford Diffraction Gemini Ultra with an ATLAS charge-coupled device (CCD) detector [$\lambda(\mathrm{MoK}\alpha) = 0.71073$ Å] at 150(2) K. Data reduction was performed using the CrysAlis software package and structure solution, and refinement was carried out using SHELXS-97 (ref. 31) and SHELXL-97 (ref. 32) using WinGX[33]. Corrections for incident and diffracted beam absorption effects were applied using analytical numeric absorption correction using a multifaceted crystal model[34].

Powder X-ray diffraction. PXRD patterns were collected on a Bruker AXS D8 powder diffractometer ($\lambda(\mathrm{CuK}\alpha) = 1.5405$ Å) equipped with a graphite monochromator in capillary mode at room temperature.

Flame atomic absorption spectroscopy analysis. FAAS analysis was performed at the Environmental Chemistry Section, Department of Chemistry, University of Glasgow, on a Perkin-Elmer 1100B atomic absorption spectrophotometer.

Flame photometry. A Corning Flame Photometer 410 at the Environmental Chemistry Section, Department of Chemistry, University of Glasgow, was used to determine the potassium and lithium content of the materials.

Thermogravimetric analysis. TGA was performed on a TA Q500 instrument under a nitrogen atmosphere. The initial heating range was from room temperature to 150 °C at 2.00 °C per min, followed by a second range from 150 °C to 1,000 °C at 5.00 °C per min.

Differential scanning calorimetry analysis. DSC analysis was performed on a TA Instruments Q 200 calorimeter under nitrogen flow at a heating rate of 20 °C min^{-1}.

Fourier-transform infrared spectroscopy. The materials were prepared as KBr pellets and FT-IR spectra were collected in transmission mode using a JASCO FT-IR-410 spectrometer. Wavenumbers (ν) are given in cm^{-1} and intensities are denoted as w = weak, m = medium, s = strong, br = broad, sh = sharp.

UV-Vis spectroscopy. Solution phase UV-Vis spectra and photometric studies were collected using a Shimadzu UV-3101PC spectrophotometer in transmission mode using quartz cuvettes with an optical path length of 1.0 cm. Solid-state UV-Vis spectra were collected on a Jasco V-670 spectrophotometer.

^{1}H-nuclear magnetic resonance spectroscopy (^{1}H-NMR). ^{1}H-NMR spectroscopy was performed on a Bruker DPX 400 spectrometer using the solvent signal as internal standard. All δ values are given in ppm.

Synthesis of $K_{18}Li_6[Mn_8(H_2O)_{48}P_8W_{48}O_{184}]\cdot 108H_2O$ (1). A 2 M aqueous LiAc solution (15 ml) was adjusted to pH 4.0 using 100% acetic acid. To this solution was then added $Mn(ClO_4)_2\cdot 2H_2O$ (102 mg, 0.4 mmol) followed by $K_{28}Li_5[H_7P_8W_{48}O_{184}]\cdot 92H_2O$ (100 mg, 7 μmol). The very pale yellow mixture was then heated at 90 °C overnight (~20 h). The mixture was slowly cooled to room temperature, transferred to a glass vial and then into a refrigerator (~4 °C); crystals began to form after one day. These well-formed pale-yellow cubic crystals were separated three days after crystallization began (yield, 52 mg, 3.28 μmol (46.4% based on tungsten)). Diffraction quality crystals were grown by the slow diffusion of methanol into the reaction mother liquor and by slow evaporation of the mother liquor over a two- to three-week period.

Characterization. Characteristic IR bands (cm^{-1}): 2,010(s), 1,628(s), 1,419(m), 1,350(w), 1,135(s), 1,080(s), 1,021(s), 953(s), 930(s). UV bands (λ (nm), ε ($\mathrm{M}^{-1}\ \mathrm{cm}^{-1}$)): 560 (2.50), 350 (4.00). Elemental analysis for the partially dehydrated material, $K_{18}Li_6[Mn_8(H_2O)_{48}P_8W_{48}O_{184}]\cdot 90H_2O$ $M_W = 15{,}688.91$ gmol^{-1}; calcd. (found, partial solvent water lost): manganese 2.80 (2.80), tungsten 56.28 (54.50), potassium 4.47 (4.52), lithium 0.28 (0.28)%. TGA water loss from 0 to 250 °C: calcd. (found), 12.14 (12.32%). Redox titrations: the cerimetric titration of a solution of compound **1** showed the presence of eight electrons, which (formally) corresponds to 8 Mn(II) centres.

X-ray diffraction structure analysis and crystallographic data. $H_{292}K_{18}Li_6Mn_8O_{340}P_8W_{48}$, $M_r = 16011.15$ g mol^{-1}; cubic crystal: 0.09 × 0.08 × 0.04 mm^3; cubic space group, $Pm\text{-}3m$, $a = b = c = 30.021(3)$ Å, $\alpha = \beta = \gamma = 90°$, $V = 27{,}057(4)$ $\mathrm{Å}^3$, $Z = 3$, $T = 150$ K, $\rho_{calcd} = 2.915$ g cm^{-3}, $\mu(\mathrm{MoK}_\alpha) = 15.856$ mm^{-1}, 23,692 reflections measured, 3,688 unique ($R_{int} = 0.1566$) of which were used in all calculations; structure solution and refinement were performed using WinGX[33]. Final $R1 = 0.0522$ and $wR2 = 0.1057$ (all data). CSD-380344 contains the supplementary crystallographic data for **1** (data available from CrysDATA@FIZ-Karlsruhe.de).

Received 11 November 2009; accepted 29 January 2010; published online 14 March 2010

References

1. Takeda, N., Umemoto, K., Tamaguchi, K. & Fujita, M. A nanometre-sized hexahedral coordination capsule assembled from 24 components. *Nature* **398,** 794–796 (1999).
2. Pluth, M. D., Bergman, R. G. & Raymond, K. N. Acid catalysis in basic solution: a supramolecular host promotes orthoformate hydrolysis. *Science* **316,** 85–88 (2007).
3. Ziv, A. *et al.* Flexible pores of a metal oxide-based capsule permit entry of comparatively larger organic guests. *J. Am. Chem. Soc.* **131,** 6380–6382 (2009).
4. Mal, P., Breiner, B., Rissanen, K. & Nitschke, J. R. White phosphorus is air-stable within a self-assembled tetrahedral capsule. *Science* **324,** 1697–1699 (2009).
5. Dinolfo, P. H. & Hupp, J. T. Supramolecular coordination chemistry and functional microporous molecular materials. *Chem. Mater.* **13,** 3113–3125 (2001).
6. Sato, S. *et al.* Fluorous nanodroplets structurally confined in an organopalladium sphere. *Science* **313,** 1273–1276 (2006).
7. Yaghi, O. M. *et al.* Reticular synthesis and the design of new materials. *Nature* **423,** 705–714 (2003).
8. Olenyuk, B., Whiteford, J. A., Fechtenkötter, A. & Stang, P. J. Self-assembly of nanoscale cuboctahedra by coordination chemistry. *Nature* **398,** 796–799 (1999).
9. Li, Q. *et al.* Docking in metal-organic frameworks. *Science* **325,** 855–859 (2009).
10. Rowsell, J. & Yaghi, O. M. Metal–organic frameworks: a new class of porous materials. *Microporous Mesoporous Mater.* **73,** 3–14 (2004).
11. Perry, J. J., Perman, P. A. & Zaworotko, M. J. Design and synthesis of metal–organic frameworks using metal–organic polyhedra as supermolecular building blocks. *Chem. Soc. Rev.* **38,** 1400–1417 (2009).
12. Kitagawa, S., Kitaura, R. & Noro, S.-I. Functional porous coordination polymers. *Angew. Chem. Int. Ed.* **43,** 2334–2375 (2004).
13. Tao, Y., Kanoh, H., Abrams, L. & Kaneko, K. Mesopore-modified zeolites: preparation, characterization and applications. *Chem. Rev.* **106,** 896–910 (2006).
14. Long, D.-L., Burkholder, E. & Cronin, L. Polyoxometalate clusters, nanostructures and materials: from self assembly to designer materials and devices. *Chem. Soc. Rev.* **36,** 105–121 (2007).
15. Müller, A. *et al.* Artificial cells: temperature-dependent, reversible Li^+-ion uptake/release equilibrium at metal oxide nanocontainer pores. *Angew. Chem. Int. Ed.* **43,** 4466–4470 (2004).

16. Geletii, Y. V. *et al.* An all-inorganic, stable and highly active tetraruthenium homogeneous catalyst for water oxidation. *Angew. Chem. Int. Ed.* **47,** 3896–3899 (2008).
17. Dolbecq, A. *et al.* Hybrid 2D and 3D frameworks based on ε-Keggin polyoxometalates: experimental and simulation. *Eur. J. Inorg. Chem.* 3009–3018 (2005).
18. Rodriguez-Albelo, L. M. *et al.* Zeolitic polyoxometalate-based metal–organic frameworks (Z-POMOFs): computational evaluation of hypothetical polymorphs and the successful targeted synthesis of the redox-active Z-POMOF1. *J. Am. Chem. Soc.* **131,** 16078–16087 (2009).
19. Müller, A., Shah, S. Q. N., Bögge, H. & Schmidtmann, M. Molecular growth from a Mo_{176} to a Mo_{248} cluster. *Nature* **397,** 47–50 (1999).
20. Schemberg, J. *et al.* Towards biological supramolecular chemistry: a variety of pocket-templated, individual metal oxide cluster nucleations in the cavity of a Mo/W-storage protein. *Angew. Chem. Int. Ed.* **46,** 2408–2413 (2007).
21. AlDamen, M. A. *et al.* Mononuclear lanthanide single-molecule magnets based on polyoxometalates. *J. Am. Chem. Soc.* **130,** 8874–8875 (2008).
22. Pope, M. T. & Müller, A. *Polyoxometalate Chemistry: From Topology via Self-Assembly to Applications* (Kluwer, 2001).
23. Pradeep, C. P., Long, D.-L., Kögerler, P & Cronin, L. Controlled assembly and solution observation of a 2.6 nm polyoxometalate 'super' tetrahedron cluster: $[KFe_{12}(OH)_{18}(\alpha\text{-}1,2,3\text{-}P_2W_{15}O_{56})_4]^{29-}$. *Chem. Commun.* 4254–4256 (2007).
24. Ritchie, C. *et al.* Reversible redox reactions in an extended polyoxometalate framework solid. *Angew. Chem. Int. Ed.* **47,** 6881–6884 (2008).
25. Uchida, S., Hashimoto, M. & Mizuno, N. A breathing ionic crystal displaying selective binding of small alcohols and nitriles: $K_3[Cr_3O(OOCH)_6(H_2O)_3][\alpha\text{-}SiW_{12}O_{40}]\cdot 16H_2O$. *Angew. Chem. Int. Ed.* **42,** 2814–2817 (2002).
26. Van Bekkum, H., Flanigen, E. M., Jacobs, P. A. & Jansen, J. C. (eds) *Introduction to Zeolite Science and Practice* (Elsevier, 2001).
27. van Bekkum, H. & Cejka, J. Zeolites and ordered mesoporous materials: progress and prospects, in *Studies in Surface Science* Vol. 157 (Elsevier, 2005).
28. Contant, R. & Teze, A. A new crown heteropolyanion, $K_{28}Li_5H_7P_8W_{48}O_{184}\cdot 92H_2O$: synthesis, structure and properties. *Inorg. Chem.* **24,** 4610–4614 (1985).
29. Müller, A. *et al.* Metal-oxide-based nucleation process under confined conditions: two mixed-valence V_6-type aggregates closing the W_{48} wheel-type cluster cavities. *Angew Chem. Int. Ed.* **46,** 4477–4480 (2007).
30. Mal, S. & Kortz, U. The wheel-shaped Cu_{20}-tungstophosphate $[Cu_{20}Cl(OH)_{24}(H_2O)_{12}(P_8W_{48}O_{184})]^{25-}$ ion. *Angew. Chem. Int. Ed.* **44,** 3777–3870 (2005).
31. Sheldrick, G. M. Phase annealing in *SHELX*-90: direct methods for larger structures. *Acta Crystallogr. A* **46,** 467–473 (1990).
32. Sheldrick, G. M. A short history of *SHELX*. *Acta Cryst. A* **64,** 112–122 (2008).
33. Farrugia, L. J. *WinGX* suite for small-molecule single-crystal crystallography. *J. Appl. Cryst.* **32,** 837–838 (1999).
34. Clark, R. C. & Reid, J. S. The analytical calculation of absorption in multifaceted crystals. *Acta Cryst. A* **51,** 887–897 (1995).

Acknowledgements

This work was supported by the EPSRC, BP Chemicals, WestCHEM, The Leverhulme Trust and The University of Glasgow. The authors would like to thank M. Beglan for assistance with FP and FAAS analysis and A. Macdonell for the concept movie showing the assembly of the cubic array.

Author contributions

S.M. and L.C. designed experiments, analysed data, prepared the figures and wrote the manuscript. C.S. provided invaluable advice and assisted with the PXRD. H.M. performed electrochemistry measurements. D.L. checked the crystallography. T.B. verified the synthesis.

Additional information

The authors declare no competing financial interests. Supplementary information accompanies this paper at www.nature.com/naturechemistry. Reprints and permission information is available online at http://npg.nature.com/reprintsandpermissions/. Correspondence and requests for materials should be addressed to L.C.